Journal of Asian Earth Sciences 34 (2009) 771–780

Contents lists available at ScienceDirect

Journal of Asian Earth Sciences

journal homepage: www.elsevier.com/locate/jaes

Disparity between measured and BSR heat flow in the Xisha Trough of the South China Sea and its implications for the methane hydrate

Lijuan He [a,*], Jiyang Wang [a], Xing Xu [b], Jinqiang Liang [b], Hongbin Wang [b], Guangxue Zhang [b]

[a] Institute of Geology and Geophysics, Chinese Academy of Sciences, P.O. Box 9825, Beijing 100029, China
[b] Guangzhou Marine Geological Survey, Guangzhou 510760, China

ARTICLE INFO

Article history:
Received 30 November 2006
Received in revised form 29 October 2008
Accepted 24 November 2008

Keywords:
Bottom-simulating reflector
Heat flow
Methane hydrate
Xisha Trough
South China Sea

ABSTRACT

We calculate the heat flow from the depth of bottom-simulating seismic reflectors (BSRs) on a seismic profile in the Xisha Trough of the South China Sea, and compare them with the probe heat flow measurements. The BSR heat flow turn out to be 32–80 mW/m^2, significantly lower than the measurements of 83–112 mW/m^2. Such big disparity cannot be ascribed only to the errors from parameters (parameter errors) that traditionally believed to influence the BSR heat flow. Besides the parameter errors, we discuss emphatically the errors coming from the theoretical assumption for the BSR heat flow determination (theoretical errors), which occur when the BSR depth does not coincide with the base of the methane hydrate stability zone (MHSZ). If BSR stays bellow the base of MHSZ, lying at the top of free gas zone, the derived heat flow would be underestimated. Compared with the parameter errors, the theoretical errors would be relatively larger in some geological settings. The disparity between measured and BSR heat flow in the Xisha Trough might be mainly due to the theoretical error. Based on the theoretical model, assuming that the BSR lying at the top of the free gas zone, the methane flux along the Xisha seismic profile is estimated, and the thickness of the methane hydrate occurrence zone is predicted.

1. Introduction

Bottom-simulating reflectors (BSRs) commonly occur several hundred meters beneath the seafloor in continental slope sediments. These reflectors were inferred to mark the base of the region for methane hydrate stability zone (MHSZ), and the heat flow derived from them is called BSR heat flow in this paper. Yamano et al. (1982) initially put forward a method which used the pressure (P)/temperature (T) relation of the gas hydrate phase change and the depth of BSR to calculate heat flow. After that, numerous studies have been made on heat flow estimates based on the BSR depth (Davis et al., 1990; Fisher and Hounslow, 1990; Hyndman et al., 1992; Ashi and Taira, 1993; Townend, 1997; Ganguly et al., 2000; Kaul et al., 2000). Regional studies of BSR heat flow have identified regional trends in several accretionary prisms, such as the Barbados (Fisher and Hounslow, 1990), Nankai (Ashi and Taira, 1993) and Cascadia (Davis et al., 1990; Hyndman et al., 1992). BSR was even used as calibration for heat flow estimates (Hyndman et al., 1992). In many cases, there is general agreement between the regional trend and BSR heat flow, and the method of heat flow calculation, might be less accurate, but much easier than the heat flow probe techniques.

However, comparisons of measured and BSR heat flow reveal that they are not always identical. For example, on the lower slope of the Cascadia accretionary prism (Davis et al., 1990), a consistent discrepancy was observed between the probe heat flow measurements and the estimates from BSR. In the Makran accretionary prism of Pakistan (Kaul et al., 2000), the estimated BSR heat flow in all basins are significantly higher than the measured values.

The discrepancy between measured and BSR heat flow was usually explained by the calculation errors from parameters, such as the applicable P/T relationship for hydrate stability, the seafloor temperature to obtain the temperature gradient, the thermal conductivity–depth relation, and the density model for the pressure at the depth of BSR. We define this kind of error as parameter error in this paper. Uncertainties coming from these factors are listed in Table 1. The cumulative effects of uncertainties in several parameters are approximately 25% by Yamano et al. (1982), 10% reported by Minshull and White (1989), and 25% by Zwart et al. (1996), 22% reported by Townend (1997), 20% by Ganguly et al. (2000), and 10% by Kaul et al. (2000).

In fact, the discrepancy might also source from the theoretical assumption for the determination of BSR heat flow that the BSR marks the base of the MHSZ. In some cases, there is general agreement between the BSR and the base of the MHSZ. However, BSR may lie at the base of the methane hydrate zone (MHZ) and wholly within the MHSZ, if the impedance contrast associated with it is produced by the seismic velocity contrast between hydrate-bearing

* Corresponding author. Tel.: +86 10 62007813; fax: +86 10 62010846.
E-mail address: ljhe@mail.igcas.ac.cn (L. He).

1367-9120/$ - see front matter © 2008 Elsevier Ltd. All rights reserved.
doi:10.1016/j.jseaes.2008.11.004

Table 1
Source and range of parameter errors.

Source	Error range (%)
Seafloor temperature	12 (Townend, 1997); negligible (Hyndman et al., 1992)
Reflection time	2 (Davis et al., 1990)
Velocity–depth relationship	<5 (Ganguly et al., 2000)
Thermal conductivity	10 (Ganguly et al., 2000)
Lithostatic/hydrostatic pressure model	8–12 (Ganguly et al., 2000)
Hydrate stability *P–T* relationship (pure water/seawater)	5 (Davis et al., 1990)
Hydrate stability *P–T* relationship (advective system)	12 (Ganguly et al., 2000)

sediments above and hydrate-free sediments below, which have been known for many regions of the world (Stoll and Bryan, 1979; Dvorkin and Nur, 1993). BSRs may sometimes occur below the MHSZ, at the top of the free gas zone (e.g., Minshull et al., 1994; Holbrook et al., 1996). Xu and Ruppel (1999) have achieved two significant results from their theoretical analysis: (1) the base of the zone in which gas hydrate actually occurs in marine sediments will not usually coincide with the base of the stability zone but rather will lie at a more shallow depth than the base of the stability zone. If the BSR represents the base of the methane hydrate-bearing layer, then the BSR may occur wholly within the MHSZ. (2) If the BSR marks the top of the free gas zone, then the BSR should occur substantially deeper than the base of the stability zone in some setting. Therefore, this basic theoretical assumption for the determination of BSR heat flow is not always proper, and may lead to errors defined as theoretical errors here.

In this paper, we firstly calculate the heat flow based on the BSR depth along a seismic profile in the Xisha Trough of South China Sea (SCS), and compare them with the probe heat flow measurements. And then, we put emphasis on the discussion of the possible factors yielding to discrepancy between the estimates and measurements, aiming to explain the difference between the measured and BSR heat flow in the Xisha Trough. Finally, we estimate the methane flux along the Xisha seismic profile based on the model of Xu and Ruppel (1999), and predict the thickness of the methane hydrate occurrence zone.

2. Background

2.1. Geological setting

The Xisha Trough (Fig. 1) situates near 18°N in the northwest of the SCS. It is located to the north of the Xisha Islands, south of the Pearl River Mouth Basin, east of the Qiongdongnan basin, and northwest of the Northwest (NW) Sub-basin of the SCS. The trough is 430 km long and 14 km wide, deepens eastwards from 1500 m to 3300 m. It is considered as a Cenozoic rift (He et al., 1980), whose evolution is closely related with the NW sub-basin, most likely had been mainly developed before 30 Ma and became a failed rift with the cease of the NW sub-basin (Shi et al., 2002). Though its neighboring area has developed igneous activities later and some faults may be active now, the Xisha Trough has substantially experienced thermal subsidence since 30 Ma, and has accumulated about 4 km of sediments in the center. The basement of the trough contains pre-Cenozoic metamorphic and granitic rocks, covered by upper Cretaceous – Quaternary sediments. The layer of upper Cretaceous to Eocene formation is 1000–5000 m thick, Oligocene – mid-Miocene formation is 500–2500 m, and upper Miocene – Quaternary formation is 200–600 m.

The Xisha Trough is adjacent to several oil–gas basins, such as the Qiongdongnan basin and the Pearl River Mouth basin. The organic carbon concentration bearing in the shallow sediments is 0.41–1.02%, showing great potential of hydrocarbon resources (Zhu et al., 2005). Since 1999, the Guangzhou Marine Geological Survey has developed several geological and geophysical investigations aiming for gas hydrate, and found many BSRs in this region. Along a seismic profile (Figs. 1 and 2), a discontinuous BSR is observed, and the heat flow are measured by the marine heat flow probe (Xu, 2005; Xu et al., 2006).

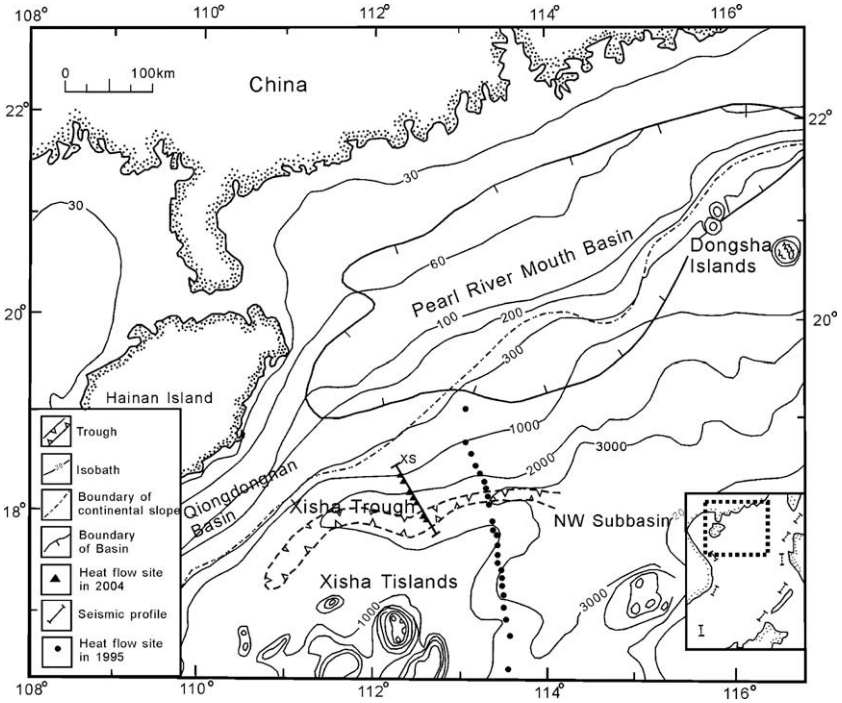

Fig. 1. Location of the Xisha Trough in the SCS.

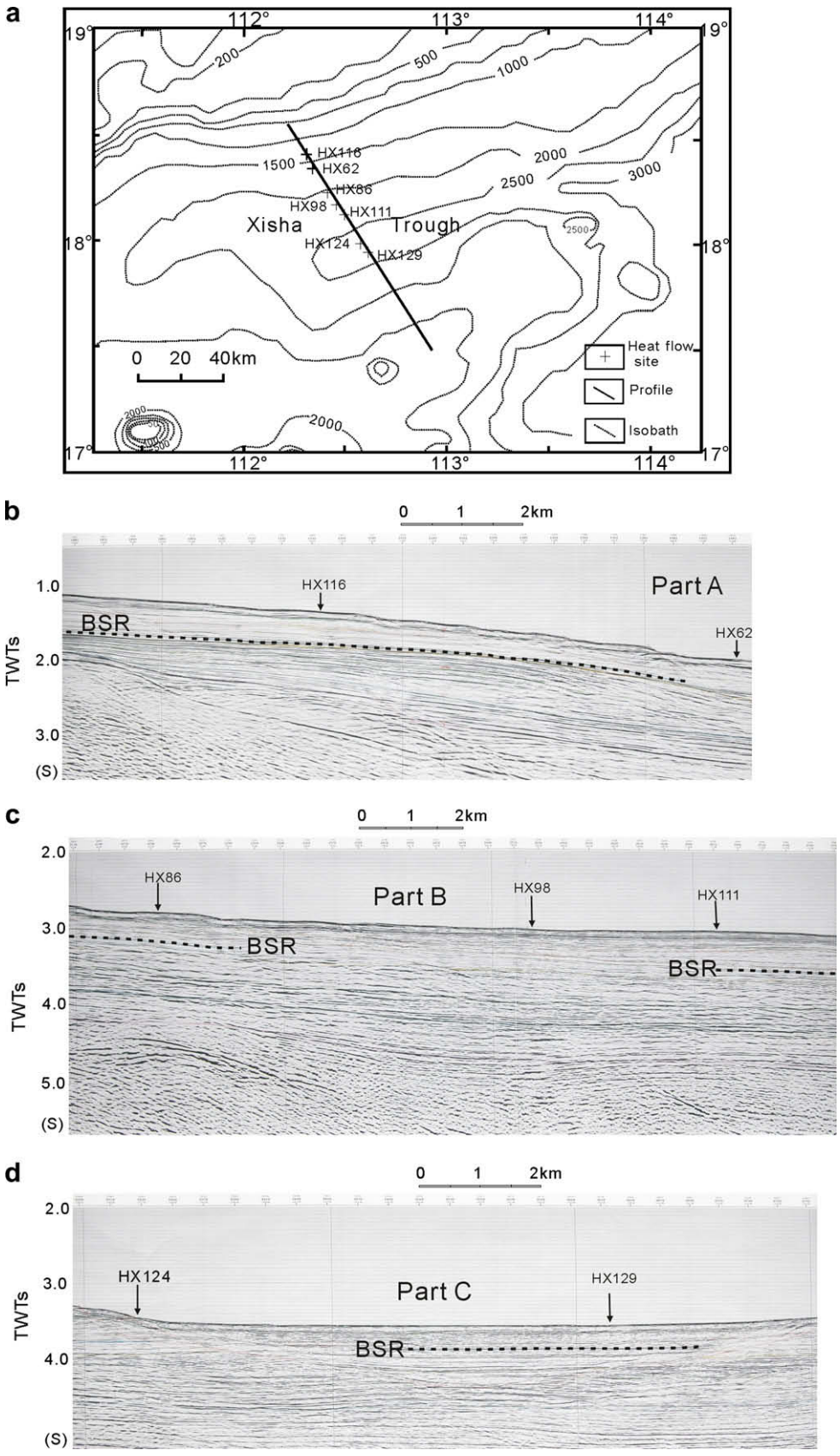

Fig. 2. Three parts of the Xisha seismic profile where BSRs are discontinuously visible. The arrows point at where the probe heat flow measurements are obtained.

2.2. Heat flow pattern

The northern South China Sea is a passive continental margin with high heat flow background of 75 mW/m^2 (He et al., 2001). Years ago, a series of probe heat flow measurements (Fig. 1) across the Xisha Trough were made jointly by PRC and USA (Nissen et al., 1995), which lied at the eastern side of the Xisha seismic profile. The heat flow measurements range from 42 to 121 mW/m^2, with an average of 80 mW/m^2. Among these data, measurements within the northern slope area and trough are generally higher than those near the Xisha Islands south of the trough. Eight heat flow measurements in the trough and its northern slope range from 70 to 121 mW/m^2 with a mean of 97 mW/m^2.

In 2004, Guangzhou Marine Geological Survey made a newest heat flow survey along the Xisha seismic profile (Xu, 2005) (Fig. 1), which is the first time especially for the methane hydrate investigation in the SCS. The miniaturized temperature data loggers (MTLs) they used are made from the Fa-Antares Company of Germany (Pfender and Villinger, 2002). The MTLs are constructed to be extremely robust, small (16 cm long) and easy to operate in water depths up to 6000 m. The temperature range extends from −5 to +60 °C with an absolute accuracy of 0.1 K. Higher absolute accuracy requires calibration with a high precision thermometer. The resolution of the A/D converter is 16 bit which leads to a temperature resolution of 0.001 K. The logging duration and sampling rate can be chosen independently. Up to 18 h of measurement are possible with the highest sample rate of 1 s. Data are stored in the non-volatile memory which holds up to 64,800 measurements. The probe is configured and data downloaded without opening the pressure case by using specialized software and interface hardware. Four or six MTLs are attached to a 6-m lance in distance of 1 m, and the temperature gradients over such depth interval can be measured. To calculate heat flow, the thermal conductivities of sediments are measured in the laboratory.

For the shallow water stations (<1000 m), water temperature corrections should be applied to the heat flow data. Nissen et al. (1995) had used the water temperature versus time data to make correction on the heat flow data of SCS. The data consist of monthly average temperatures at 19 standard depths from the surface to 1000 m. Monthly average bottom temperature values were calculated and used to determine Fourier series coefficients which in turn were used to calculate temperature perturbations at the depths of the temperature probes. Thermal diffusivities were determined from the thermal conductivity measurements made on piston cores raised from nearby. In general, the maximum temperature corrections are small, considerably less than the measured perturbations to linear temperature–depth gradients (Nissen et al., 1995). In this study, the water depths of heat flow sites are greater than 1000 m, and therefore the effects can be neglected.

Seven heat flow measurements (Table 2) were achieved along the seismic profile (Fig. 2a). Among them, HX129 and HX124 locate at the plain of the trough, and the others locate at the northern slope. The heat flow values vary between 83 and 112 mW/m^2. The average value turns out to be 96 mW/m^2, exhibiting a high heat flow background.

Table 2
Heat flow measurements in the Xisha Trough (from Xu et al., 2006).

Sites	E. longitude	N. latitude	Water depth (m)	Thermal gradient (°C/km)	Thermal gradient (W/m K)	Heat flow (mW/m^2)
HX129	112.623°	17.942°	2644	94	0.89	83
HX124	112.585°	17.984°	2646	91	1.06	96
HX111	112.505°	18.117°	2334	104	0.89	93
HX98	112.465°	18.167°	2264	105	0.99	103
HX86	112.423°	18.222°	2060	109	0.87	94
HX62	112.356°	18.339°	1634	107	1.05	112
HX116	112.321°	18.401°	1239	85	1.05	89

3. BSR heat flow

The Xisha seismic profile crosses through the Xisha Trough with the water depth of 1200–2700 m and seafloor temperature (T_{sea}) of 2.3–3.7 °C. The BSRs are discontinuously visible along three parts of this profile (Fig. 2b–d). Depth to BSR can be determined with Two-way travel times (TWTs) by the depth–time relationship (Wang et al., 2005):

$$z = 982.576 \times t \quad (t \leqslant 0.5\ \text{s}) \tag{1}$$

$$z = 121.52 \times t^2 + 1269.1 \times t - 173.692 \quad (1\ \text{s} \leqslant t > 0.5\ \text{s}) \tag{2}$$

where t is the TWT from seafloor, and z is the depth below seafloor.

The calculated depth to BSR is 330–460 mbsf along profile part A, 360–530 mbsf along profile part B and about 300 mbsf along profile part C.

The BSR heat flow (H_{BSR}) is calculated by the following equation (Ganguly et al., 2000):

$$H_{BSR} = k\frac{T_{BSR} - T_{sea}}{Z_{BSR}} \tag{3}$$

where T_{BSR} is the temperature at the BSR depth (Z_{BSR}), which is determined from the P–T stability conditions for methane hydrate in seawater (Miles, 1995):

$$P = 2.8074023 + aT + bT^2 + cT^3 + dT^4 \tag{4}$$

where T is the temperature in °C and P is the pressure in MPa; $a = 1.559474 \times 10^{-1}$; $b = 4.8275 \times 10^{-1}$; $c = -2.78083 \times 10^{-3}$ and $d = 1.5922 \times 10^{-4}$.

An empirical expression giving the average thermal conductivity (k) from the surface was adopted from Davis et al. (1990):

$$k = 1.07 + 5.86 \times 10^{-4} \times z - 3.24 \times 10^{-7} \times z^2 \tag{5}$$

where k is the thermal conductivity in W/m K and z is the depth below the seafloor in m. This relationship was developed by Davis et al. (1990) using the simple geometric mean (e.g., Woodside and Messmer, 1961; Sass et al., 1971), with a pore fluid conductivity of 0.60 and a matrix conductivity of 2.4 W/m K. The latter is the values used by Nobes et al. (1986) which agrees with the value for clay-rich sediments (Henderson and Davis, 1983). This value, along with the computed porosity, gives a surface conductivity of 1.07 W/m K, which is in agreement with the measurements (1.0 W/m K) in the sediments lying beneath the few meter thick hemipelagic layer in the Xisha Trough of SCS (Xu et al., 2006). The relation is generally consistent with mean values from ODP sites 1148 of SCS (Wang et al., 2000), although the latter have about 10% scatter, which probably represents a maximum estimate of error for thermal conductivity measurements (Fig. 3).

For profile part A, the BSR heat flow is determined to be 35–55 mW/m^2 (Fig. 4a), indicating a rater low heat flow regime. In contrast, the measured heat flow in HX116 is as high as 89 mW/m^2. The error between measured and BSR heat flow reaches 54%.

For profile part B, the BSR heat flow turns out to be 51–65 mW/m^2 (Fig. 4b), also showing rather low heat flow characteristic. There are three probe measurements along the section, HX86, HX98, HX111, with values of 94, 103 and 93 mW/m^2, respectively. The error between measured and BSR heat flow is 34% at point HX86, 46% at point HX111.

For profile part C, the BSR heat flow is 85 mW/m^2 (Fig. 4c), which is similar as the probe measurement of 83 mW/m^2 at point HX129.

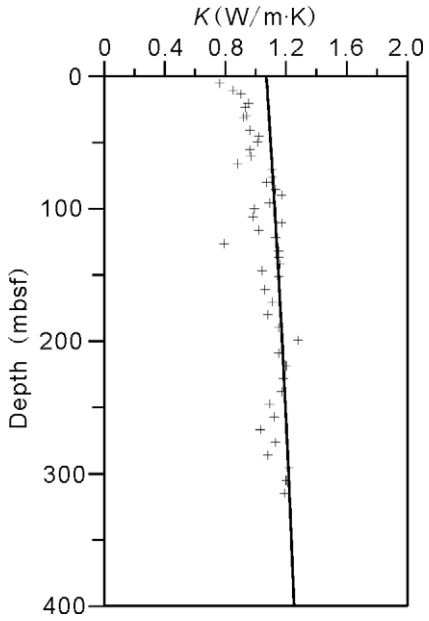

Fig. 3. Variation of thermal conductivity with depth below seafloor. The '+' indicates actual ODP site 1184 measurements (Wang et al., 2000), while the solid curve represents average conductivities measures from the surface, as determined by the relationship of Davis et al. (1990).

4. Parameter errors

Parameter error is a possible source leading to the discrepancy between estimated and measured heat flow. In our calculation, three factors affecting BSR heat flow could not be ignored (error >5%), including, (1) the thermal conductivity, (2) the pressure at the depth of BSR (lithostatic/hydrostatic pressure model) and (3) the applicable pressure–temperature relationship.

The thermal conductivity utilized in our calculation is from Davis et al. (1990), which is an empirical expression of average values from the surface. The thermal conductivity of the seafloor derived from it is 1.07 W/m K, which is a slightly bigger than the measured value of 1.0 W/m K from the samples collected 2–3 mbsf along the seismic profile in the Xisha Trough. Upon the Davis' equation, the average thermal conductivity of the sediments from surface to 500 m is predicted to be 1.28 W/m K. Such prediction is generally (~10%) greater than those from ODP leg 184 in the SCS (Fig. 3). Therefore, the Davis' equation may probably lead to slight overestimates of BSR heat flow in the Xisha Trough, and thus cannot explain the lower of estimates than the measurements.

Up to now, it is still not clear which is the more accurate density model (hydrostatic or lithostatic) for the BSR heat flow estimates (Ganguly et al., 2000), although Hyndman et al. (1992) argued that since substantial over-pressures are unlikely at the shallow BSR sub-bottom depth and it is reasonable to use the hydrostatic model. Both of the two density models have been used in previous estimates of BSR heat flow, and estimates using the hydrostatic assumption would be slightly smaller. The difference between the two models is increasing with the decreasing of water depth, since at shallower depth the fractional contribution of the sediment grains to the total pressure at the BSR depth, with respect to the contribution of the water column, is greater. In this study, we assumed hydrostatic pressure at the BSR. Compared with lithostatic assumption, the estimated heat flow using the hydrostatic assumption is only 3% smaller in profile part C, 6% smaller in profile part B and 12% smaller in profile part A. The hydrostatic model may

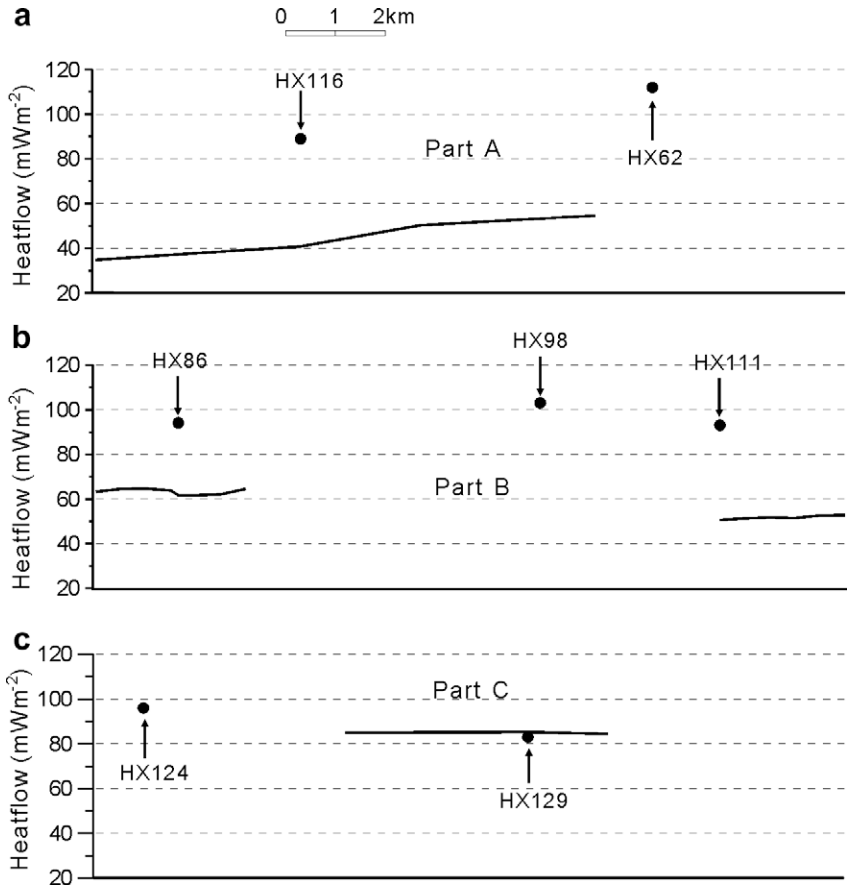

Fig. 4. Comparison between the measured and BSR heat flow. The BSR heat flow is indicated by solid curve and the probe measurements by dots in (a), (b) and (c).

lead to slight underestimate of BSR heat flow, but which is much smaller than the big discrepancy between measured and BSR heat flow in this region.

The applicable pressure–temperature relationship is another factor leading to the uncertainty of BSR heat flow. In an advective system or in a system where significant capillary effects exist, the theoretical stability curve may not be applicable (Ruppel, 1997; Xu and Ruppel, 1999) and the temperature at the BSR depth may be several degrees lower than the theoretical value (Ganguly et al., 2000). Ganguly et al. (2000) pointed out that heat flow could be systematically overestimated by 12% in this case. So, it is not the factor resulting in the lower of heat flow estimates in the Xisha Trough.

In summary, both the thermal conductivity and the pressure–temperature relation would overestimate the heat flow, and only the density model underestimate the BSR heat flow in our calculation for the Xisha Trough. Obviously, the significantly smaller of estimates than the measurements in the Xisha Trough cannot be explained by the parameter errors, other important effects must exist influencing the estimates of BSR heat flow.

5. Theoretical errors

BSR may mark the top of the free gas zone, and the BSR should occur substantially deeper than the base of MHSZ in some settings (Xu and Ruppel, 1999). In this case, BSR heat flow would be lower than the probe heat flow measurements (Fig. 5). In the Xisha Trough, the fact that the BSR heat flow greatly lower than the regional heat flow suggests that the BSR may occur below the MHSZ, at the top of free gas zone, and the disparity between the measures and BSR heat flow may source from the theoretical errors. In this study, we calculate the base of MHZ, and the top of the free gas zone based on the model of Xu and Ruppel (1999) to evaluate the theoretical error.

5.1. Method

Xu and Ruppel (1999) modeled the gas hydrate system as consisting of two components and three phases. Water and methane gas constitute the system components, while gas hydrate (subscript h), free gas (g) and water plus dissolved methane (l) represent the three phases. The fundamental equations governing the two-component, three-phase system in porous sediments are conservation of momentum fluid mass, energy and methane gas. In most cases up to two phases (hydrate and liquid) may be present above the base of the MHSZ, but only liquid is mobile. Owing to the relatively slow rate of gas hydrate formation and dissociation in most natural systems, they assumed that the pressure and temperature variations associated with its formation and accumulation are to first order negligible compared to total mass and heat transport in the system. This assumption renders the system steady state under certain boundary conditions. For simplicity, they also assumed that the amount of hydrate in pore space is sufficiently small that the liquid phase occupies almost the entire available porosity. With these assumptions the governing equations for the one-dimensional system become as:

$$q_f = -\frac{k\rho_l}{\mu_l}\left[\frac{dp}{dz} + \rho_l g\right] \tag{6}$$

$$q_e = q_f C_l T - \lambda \frac{dT}{dz} \tag{7}$$

where q_f and q_e are constant fluxes of total mass and energy, respectively, and z is the spatial coordinate that originates at the seafloor and points upward. Parameters k, ρ, μ, g, C and λ represent sediment permeability, density, dynamic viscosity, gravitational acceleration, specific heat capacity and effective thermal conductivity, respectively. In general, the bulk mass fraction of methane cannot be viewed as steady state during the formation and accumulation of hydrates. However, owing to the absence of free gas and the immobility of gas hydrate, all methane transport occurs within the liquid phase, and the steady state methane transport can be described as:

$$q_m = q_l M_l - \phi K_m S_l \frac{dM_l}{dz} \tag{8}$$

where M denotes mass fraction of methane in individual phases and K_m represents the product of the dispersion–diffusion coefficient D_m and the representative fluid density of the system, which can nominally be taken as 1000 kg/m^3 for the sake of converting between K_m and D_m. ϕ denotes the sediment porosity. The volume saturation of liquid $S_l = 1$ and q_m represents depth-dependent methane flux, which is not a constant within the MHZ. Below the base of the MHZ, q_m is a constant given by the corresponding boundary condition. Above the top of the MHZ, $q_m(z)$ reduces to a constant q_{mt}, which corresponds to the methane gas flux at the top boundary of the MHZ. The methane mass fraction in liquid is steady state but does vary spatially within the MHZ.

The locations of the base and top of MHZ can be determined by combining steady state profiles of the mass fraction of dissolved methane in sea water with system pressure and temperature

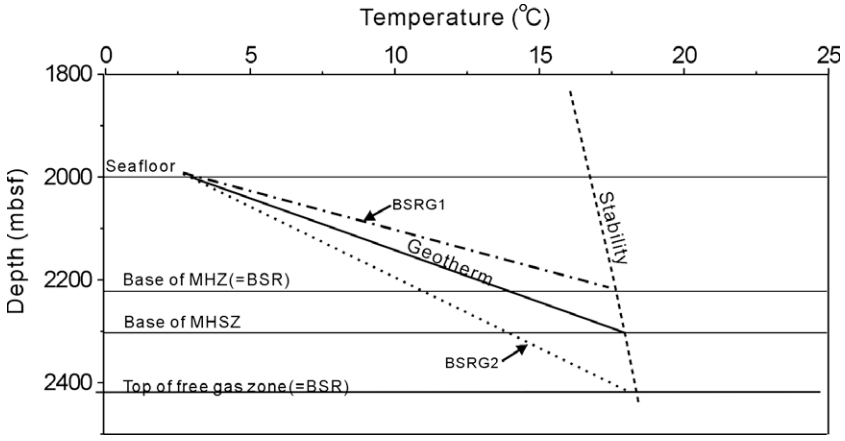

Fig. 5. Diagram showing the contrast of the regional and BSR thermal gradient. BSRG1 represents the estimated thermal gradient when the BSR designates the base of the MHZ, and BSRG2 represents the estimated thermal gradient when the BSR designates the top of the free gas zone.

parameters. Above the top of the MHZ, methane transport is described by Eq. (8), with constant $q_m(z)$ equal to q_{mt} at the top of the MHZ. Integrating Eq. (8) from the top of MHZ ($z = z_{lt}$) to the seafloor, where methane mass fraction in seawater is M_0, yields for different q_f values:

$$z_{lt} = -\frac{\phi K_m}{q_{mt}} \ln\left[\frac{q_{mt} - q_f M_0}{q_{mt} - q_f M_{sl}(z_{lt})}\right] \quad q_f \neq 0 \tag{9a}$$

$$z_{lt} = -\frac{\phi K_m}{q_{mt}} [M_{sl}(z_{lt}) - M_0] \quad q_f = 0 \tag{9b}$$

In Eq. (9),

$$q_{mt} = q_f M_{st}(z_{lt}) - \phi K_m \left[\frac{dM_{sl}}{dz}\right]_{z=z_{lt}} \tag{10}$$

Knowing methane solubility M_{st} as a function of z (or p and T), the position of the top of the MHZ (z_{lt}) can be calculated from Eq. (9) for the steady state, two-phase system. The base of the MHZ (z_{lb}) may often be shallower than the base of MHSZ ($z_{lb} > z_{sb}$) due to the dependence of z_{lb} on the rate of methane supply. The location z_{lb} of the base of MHZ can be determined iteratively using

$$q_m = q_f M_{sl}(z_{lb}) - \phi K_m \left[\frac{dM_{sl}}{dz}\right]_{z=z_{lb}} \tag{11}$$

Applying Eqs. (10) and (11) together yields the thickness of the MHZ.

The analytical model developed by Xu and Ruppel (1999) provides a means for estimating the depth to both the top of the free gas zone and the base of the MHZ in marine hydrate provinces and

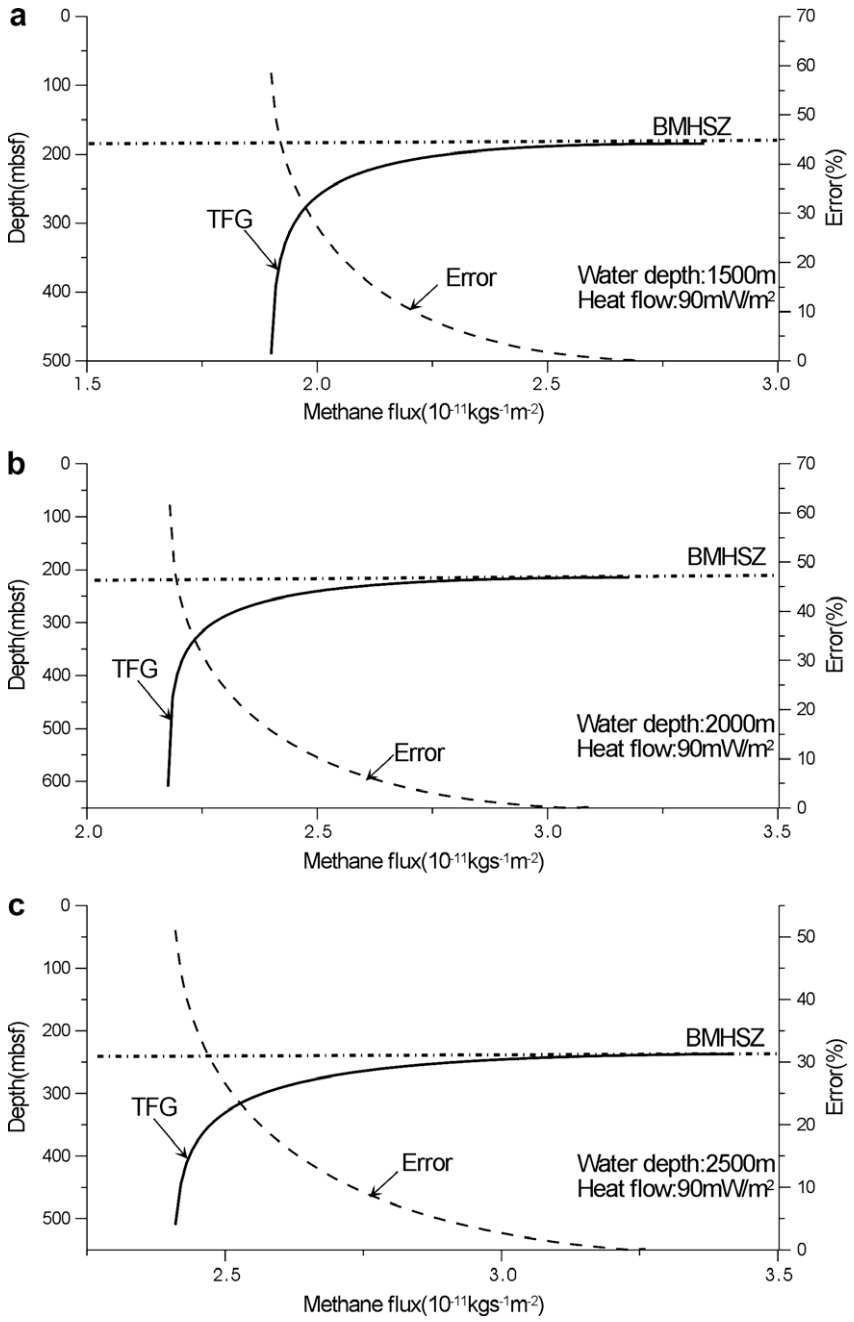

Fig. 6. The top of free gas zone (solid curve) as a function of methane flux and corresponding theoretical error when BSR marks the top of free gas zone at constant heat flow of 90 mW/m^2, and water depth of (a) 1500 m, (b) 2000 m and (c) 2500 m. TFG: top of the free gas zone; BMHSZ: base of the methane hydrate stability zone.

may thus help to constrain the nature of the BSR in real settings. The position of the top of the free gas zone can be determined using an expression similar to Eq. (9) and assuming that the methane gas solubility for the region below the base of the MHSZ can be approximated as a constant $M_{sl} = M_{sl}(z_{sb})$ (Zatsepina and Buffett, 1997).

5.2. Results

Methane flux is the key factor controlling the top of the free gas zone. An increase in methane flux may lead to shoaling of the top of the free gas zone. We calculate the variations of the depth of the top of free gas zone with changing methane flux at given water depth and heat flow (Figs. 6 and 7). The thermal conductivity is taken as 1.2 W/m K, seafloor temperature 2.4 °C, and the other parameters (Table 3) are flowing Xu and Ruppel (1999). The corresponding error $((H_{BSR} - H)/H)$ of BSR heat flow is also calculated. As H_{BSR} is smaller than H, the error is a negative value. We take the absolute value of it as the theoretical error. The first panel of Fig. 6 shows that, the top of the free gas zone goes upward as the methane flux increases and approaches the base of the MHSZ if the methane flux is greater than 2.7×10^{-11} kg/s m^2 when water depth is 1500 m and heat flow 90 mW/m^2. If the BSR marks the top of free gas zone, the BSR heat flow would be consequently underestimated, and the theoretical error increases as the methane flux decreases, with maximum error of lager than 60%.

Fig. 6b and c shows the results when the heat flow fixed but the water depth increases to 2000 m and 2500 m, respectively.

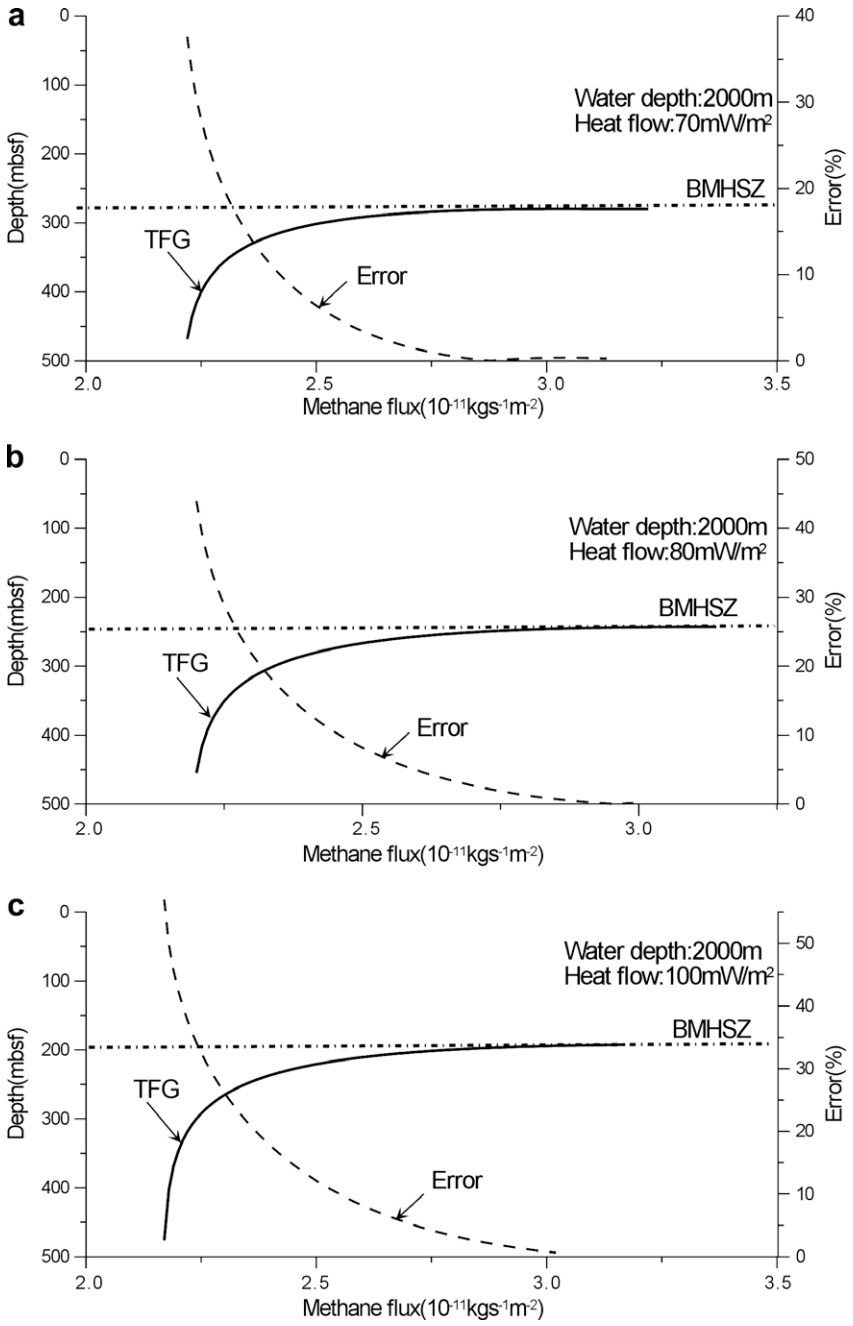

Fig. 7. The top of free gas zone (solid curve) as a function of methane flux and corresponding theoretical error when BSR marks the top of free gas zone at constant water depth of 2000 m, and heat flow of (a) 70, (b) 80 and (c) 100 mW/m^2.

Table 3
Parameters used in the model.

Parameter	Definition	Value
g	Gravitational acceleration	9.81 m/s^2
μ_l	Viscosity of liquid	8.87×10^{-4} kg/m s
q_f	Mass flux	10^{-8} kg/m^2 s
ϕ	Porosity	0.5
k	Permeability	1.0×10^{-14} m^2
D_m	Dispersion–diffusion coefficient	1.3×10^{-9} m^2/s
ρ_l	Density of liquid	1024 kg/m^3
C_l	Specific heat capacity of liquid	4180 J/kg K

Although both figures indicate the similar trend of the top of the free gas zone and corresponding error, the range of methane flux differs in different cases. Therefore, for same value of methane flux, the theoretical error is different at different geological setting, this is because the shallower the water depth, the less methane flux needed for the top of gas zone to coincide with the base of MHSZ at given heat flow. For example, when the methane flux is 2.5×10^{-11} kg/s m^2, the theoretical error is negligible when water depth is 1500 m, but it increases to 12% and 27% when water depth increases to 2000 m and 2500 m, respectively.

Fig. 7 shows the results when the water depth fixed but the heat flow varied. We can observe the similar curves exhibiting the variation of the top of the free gas zone and the theoretical error. In such case, the larger the heat flow, the larger methane flux needed for the top of the free gas zone to approach the base of MHSZ. In other words, for areas with the same methane flux value, the BSR heat flow is probably highly underestimated where the regional heat flow is high, with maximum error of more than 50%.

The results imply that, the large disparity between BSR and observed heat flow in the Xisha Trough is probably due to the disaccord between BSR depth and the base of MHSZ. The lower of BSR heat flow than the regional trend may owe to the deeper of BSR than the base of the MHSZ, suggesting BSR may mark the top of free gas zone in this trough.

6. Implications for the methane hydrate zone

The disparity between the BSR heat flow and the probe heat flow measurements implies the disaccord between the BSR depth and the base of MHSZ in the Xisha Trough. Because the disagreement between BSR depth and the base of MHSZ is mainly controlled by the value of methane flux, the comparison between the BSR heat flow and the measurements can therefore provide the information of methane flux in the region, which is important for the methane hydrate formation and distribution.

The following procedure is exploited to infer the methane flux rates at two sites in the Xisha Trough, SCS. Firstly, we give a variable value of methane flux to determine the top of the free gas zone for given water depth and heat flow. Secondly, comparing the top of the free gas zone with the depth of BSR, we can obtain the value of methane flux when the two depths are coincident. Finally, using this value of methane flux, we can then predict the thick of the MHZ.

Here, we take the Xisha seismic profile part B as example. Near point HX86, the BSR depth is 370–390 mbsf, water depth is 2060 m, and the probe heat flow measurement is 94 mW/m^2. Based on the model of Xu and Ruppel (1999), the base of MHSZ is about 207 mbsf, rather shallower than the BSR depth. If the BSR depth represents the top of the free gas zone, then the methane flux can be derived as 2.23×10^{-11} kg/s m^2 (Fig. 8) from the model of Xu and Ruppel (1999). The bottom of methane hydrate occurrence zone is predicted to be 162 mbsf, and the top of methane hydrate occurrence zone to be 80 mbsf. Consequently, the thickness of methane hydrate occurrence zone is 82 m (Fig. 8).

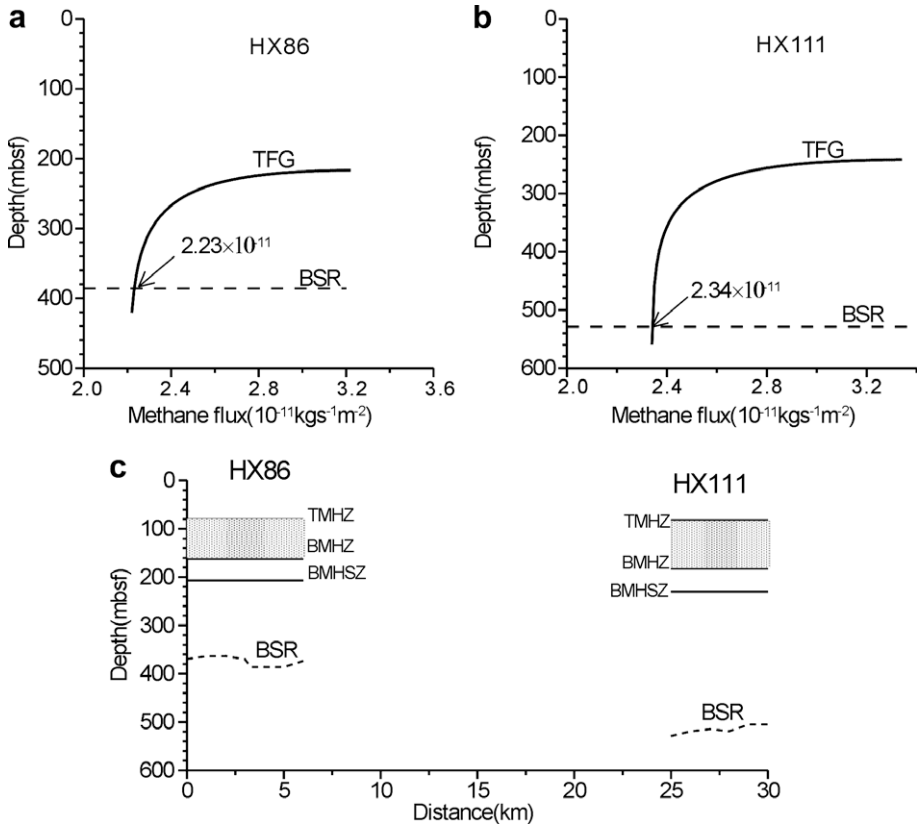

Fig. 8. Model predicted methane flux and the thickness of MHZ in the Xisha Trough along seismic profile part B.

Near point HX111, the BSR depth is 500–530 mbsf, water depth is 2334 m, and the probe heat flow measurement is 93 mW/m^2. Model results show, the bottom of methane hydrate stability zone is 230 mbsf. Using BSR depth as the top of the free gas zone, the methane flux is predicted to be 2.34×10^{-11} kg/s m^2 (Fig. 8). The bottom of methane hydrate occurrence zone is 183 mbsf, and the top of it is 82 mbsf. Thus, the thickness of methane hydrate occurrence zone is 101 m (Fig. 8).

7. Conclusion

(1) Disparity between the measured and BSR heat flow could attribute to both parameter errors and theoretical errors. The parameter errors are usually less than 25%, but the theoretical could exceed 50% in some settings.
(2) When BSR does not coincide with the base of MHSZ, the theoretical errors would occur. If BSR equals the base of MHZ, the BSR heat flow would be overestimated. If BSR stays at the top of free gas zone, the BSR heat flow would be underestimated.
(3) The estimates of BSR heat flow in the Xisha Trough of the South China Sea vary between 32 and 80 mW/m^2, which are significantly lower than the measured values of 83–112 mW/m^2. The large disparity between the measured and BSR heat flow in the Xisha Trough could not be explained only by the parameter error, but probably due to the theoretical error. The fact the BSR heat flow greatly lower than the regional heat flow in this trough suggest the BSR may mark the top of the free gas, which is lower than the base of MHSZ.
(4) Based on the model of Xu and Ruppel (1999), assuming that the BSR lying at the top of the free gas zone, the methane flux along the Xisha seismic profile part B is estimated to be $2.21–2.33 \times 10^{-11}$ kg/s m^2, and the thickness of the methane hydrate occurrence zone is 82–101 m.

Acknowledgements

The research is funded by the NSFC Project (40774033), 863 (2006AA09A203) and GZH2002002030204. We thank Dr. W. Xu very much for using his software to determine the base of MHZ and top of the free gas zone.

References

Ashi, J., Taira, A., 1993. Thermal structure of the Nankai accretionary prism as inferred from gas hydrate BSRs. In: Underwood, M.B. (Ed.), Thermal Evolution of the Tertiary Shimanto Belt, Southwest Japan: An Example of Ridge–Trench Interaction, vol. 273, pp. 137–149.
Davis, E.E., Hyndman, R.D., Villinger, H., 1990. Rates of fluid expulsion across the northern Cascadia accretionary prism: constraints from new heat flow and multichannel seismic reflection data. J. Geophys. Res. 95, 8869–8889.
Dvorkin, J., Nur, A., 1993. Rock physics for characterization of gas hydrates. In: The Future of Energy Gases. US Geol. Surv. Prof. Pap. 1570, 293–298.
Fisher, A.T., Hounslow, M.W., 1990. Transient fluid flow through the toe of the Barbados accretionary complex: constraints from ODP Leg 110 heat flow studies and simple models. J. Geophys. Res. 95, 8845–8858.
Ganguly, N., Spence, G.D., Chapman, N.R., Hyndman, R.D., 2000. Heat flow variations from bottom simulating reflectors on the Cascadia margin. Mar. Geol. 164, 53–68.
He, L.S., Wang, G.Y., Shi, X.C., 1980. Xisha Trough—a Cenozoic rift. Geol. Rev. 26 (6), 486–489 (in Chinese).
He, L., Wang, K., Xiong, L., Wang, J., 2001. Heat flow and the thermal history of the South China Sea. Phys. Earth Planet Int. 126, 211–220.
Henderson, J., Davis, E.E., 1983. An estimate of the heat flow in the western North Atlantic at Deep Sea Drilling Project site 534, Initial Report. Deep Sea Drill. Proj. 76, 719–724.
Holbrook, W.S., Hoskins, H., Wood, W.T., Stephen, R.A.Lizarralde, Leg 164 Science Party, 1996. Methane hydrate and free gas on the Blake Ridge from vertical seismic profiling. Science 273, 1840–1843.
Hyndman, R.D., Foucher, J.P., Yamano, M., Fisher, A., 1992. Scientific Team of Ocean Drilling Program Leg 131, Deep sea bottom-simulating-reflectors: calibration of the base of the hydrate stability field as used for heat flow estimates. Earth Planet Sci. Lett. 109, 289–301.
Kaul, N., Rosenberger, A., Villinger, H., 2000. Comparison of measured and BSR-derived heat flow values, Makran accretionary prism. Pakistan Mar. Geol. 164, 37–51.
Miles, P.R., 1995. Potential distribution of methane hydrate beneath the European continental margins. Geophys. Res. Lett. 22, 3179–3182.
Minshull, T., White, R., 1989. Sediment compaction and fluid migration in the Makran accretionary prism. J. Geophys. Res. 89, 11549–11559.
Minshull, T.A., Singh, S.C., Westbrook, G.K., 1994. Seismic velocity structure at a gas hydrate reflector, offshore western Colombia, from full waveform inversion. J. Geophys. Res. 99, 4715–4734.
Nissen, S.S., Hayes, D.E., Yao, B., 1995. Gravity heat flow, and seismic constraints on the processes of crustal extension: northern margin of the South China Sea. J. Geophys. Res. 100 (B11), 22447–22483.
Nobes, D.C., Viilinger, H., Davis, E.E., Law, L.K., 1986. Estimation of marine sediment bulk physical properties at depth from seafloor geophysical measurements. J. Geophys. Res. 91, 14033–14043.
Pfender, M., Villinger, H., 2002. Miniaturized data loggers for deep sea sediment temperature gradient measurements. Mar. Geol. 186, 557–570.
Ruppel, C., 1997. Anomalously cold temperatures observed at the base of gas hydrate stability zone on the US Atlantic passive margin. Geology 25, 699–702.
Sass, J.H., Lachenbruch, A.H., Munroe, R.J., 1971. Thermal conductivity of rocks from measurements on fragments and its application to heat flow determinations. J. Geophys. Res. 76, 3391–3401.
Shi, X., Zhou, D., Qiu, X., Zhang, Y., 2002. Thermal and rheological structures of the Xisha Trough, South China Sea. Tectonophysics 351, 285–300.
Stoll, R.D., Bryan, G.M., 1979. Physical properties of sediments containing gas hydrates. J. Geophys. Res. 84, 1629–1634.
Townend, J., 1997. Estimates of conductive heat flow through bottom-simulating reflectors on the Hikurangi and southwest Fiordland continental margins, New Zealand. Mar. Geol. 141, 209–220.
Wang, P., Prell, W.L., Blum, P., 2000. In: Proceedings of the ODP, Initial Reports 184, College Station TX (Ocean Drilling Program).
Wang, H., Liang, J., Gong, Y., 2005. Estimation of the heat flow in the Northern of the South China Sea based on the seismic data of gas hydrate. Geoscience 19, 67–73 (in Chinese).
Woodside, W., Messmer, J.H., 1961. Thermal conductivity of porous media. J. Appl. Phys. 32, 1688–1699.
Xu, X., 2005. The marine heat flow survey and the result discussion in the northern part of South China Sea. Progress in Geophysics 20, 562–565 (in Chinese).
Xu, W., Ruppel, C., 1999. Predicting the occurrence, distribution, and evolution of methane gas hydrate in porous sediments. J. Geophys. Res. 104, 5081–5095.
Xu, X., Shi, X., Luo, X., Liu, F., Guo, X., Sha, Z., Yang, X., 2006. Marine heat flow measurements in the Xisha Troufh, South China Sea. Marine Geology and Quaternary Geology 26, 51–57.
Yamano, M., Uyeda, S., Aoki, Y., Shipley, T.H., 1982. Estimates of heat flow derived from gas hydrates. Geology 10, 339–343.
Zatsepina, O., Buffett, B.A., 1997. Phase equilibrium of gas hydrate: Implications for the formation of hydrate in the deep sea-floor. Geophys. Res. Lett. 24, 1567–1570.
Zhu, Y., Rao, Z., Liu, J., Liu, Y., Bai, R., 2005. Geochemical anomalies and their implication from site 14, the Xisha Trough, the South China Sea. Geoscience 19, 39–44 (in Chinese).
Zwart, G., Moore, J.C., Cochrane, G.R., 1996. Variations in temperature gradients identify active faults in the Oregon accretionary prism. Earth Planet Sci. Lett. 139, 485–495.